Front. Environ. Sci. Eng. 2021, 15(4): 53
https://doi.org/10.1007/s11783-020-1345-7

RESEARCH ARTICLE

Characterization of electrode fouling during electrochemical oxidation of phenolic pollutant

Xuefeng Liu[1], Shijie You (✉)[1], Fang Ma[1], Hao Zhou[2]

1 State Key Laboratory of Urban Water Resource and Environment, Harbin Institute of Technology, Harbin 150090, China
2 Conservation Center, Shanghai Museum, Shanghai 200231, China

HIGHLIGHTS

- Electrode fouling is characterized by non-destructive characterization.
- Electrode fouling is highly dependent on electrochemical process.
- Active chlorine can prevent the formation of polymeric fouling film.

GRAPHIC ABSTRACT

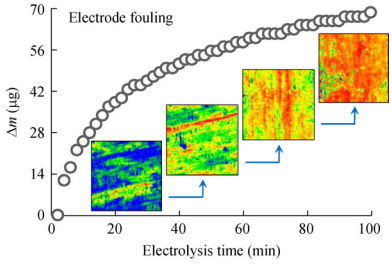

ARTICLE INFO

Article history:
Received 29 April 2020
Revised 17 June 2020
Accepted 22 July 2020
Available online 9 October 2020

Keywords:
Electro-oxidation
Electrode fouling
Polymeric film
Chloride ions

ABSTRACT

Electrode fouling is a problem that commonly occurs during electro-oxidation water purification. This study focused on identifying the fouling behavior of Pt electrode associated with the formation of polymeric layer during electro-oxidation of phenol. The in situ electrochemical measurements and non-destructive observation of the electrode morphology were reported. The results demonstrated that the electrode fouling was highly dependent on thermodynamic process of electrode that was controlled by anode potential. At anode potential lower than 1.0 V vs SHE, the direct electro-oxidation caused the electrode fouling by the formation of polymeric film. The fouling layer decreased the electrochemically active surface area from 8.38 cm^2 to 1.57 cm^2, indicated by the formation of polymeric film with thickness of 2.3 μm, increase in mass growing at a rate of 3.26 μg/cm^2/min. The degree to which the anode was fouled was independent of anion in the electrolyte. In comparison, at anode potential higher than 2.7 V vs SHE, the anions (e.g., chloride) could exert a major influence to the behavior of electrode fouling. The presence of chloride was shown to mitigate the fouling of electrode significantly through preventing the formation of polymeric film by active chlorine (e.g., Cl• and Cl_2) produced from anodic oxidation of chloride. Since chloride is the most abundant anionic species existing in both natural and engineered water system, this study not only offers a deep insight into the mechanism of electrode fouling, but also suggests strategies for anti-fouling in the presence of chloride in electro-oxidation process.

1 Introduction

Electrochemical oxidation represents a prominent technology in the widespread of application of decentralized water and wastewater purification (Martínez-Huitle and Ferro, 2006; Wang et al., 2020). As electrons play a role of clean reagent, electrochemical wastewater purification has become competitive by its efficient and environmentally compatible process (Tang et al., 2014; Xu et al., 2018; Qi et al., 2020). However, electrode fouling on the anode surface impedes the practical applications of electrochemical oxidation. For example, the electro-oxidation of organic compounds on a boron-doped diamond (BDD) electrode leads to a decrease in current decay of more than 80% from the initial 4.1 mA/cm^2 to the steady-state 0.6 mA/cm^2 due to the formation of polymeric film on the electrode surface during long-term operation (Iniesta et al., 2001).

According to previous reports, the major causes of electrode fouling are attributed to the electro-oxidation of phenolic compounds and formation of a passivating film on the electrode surface (Gattrell and Kirk, 1992; Ferreira

✉ Corresponding author
E-mail: sjyou@hit.edu.cn

et al., 2006; Gao and Vecitis, 2012). When using electrochemical oxidation to treat realistic wastewater containing similar species such as sulfamethazine (Barhoumi et al., 2016), tetrabromobis phenol A (Hou et al., 2018), tetracycline (Barhoumi et al., 2017), phenacetin (Xiao and Zhang, 2016) and orange G dye (Almeida et al., 2015), these compounds can be oxidized to produce phenolic compounds that potentially trigger electrode fouling.

In addition to organic pollutants themselves, the anions (e.g., Cl^-, SO_4^{2-}) in realistic wastewater at concentration in a wide range from hundreds (surface water) to thousands (industrial wastewater) of milligrams per liter may constitute important factor that affects the electrode fouling. In electrochemical advanced oxidation process, oxidation is mainly mediated by active intermediates like hydroxyl radicals (OH•) and active chlorine (e.g., Cl•, Cl_2, HClO). So far, a number of studies investigated the electrode fouling in the inert electrolyte. For example, Iniesta et al. reported the BDD electrode could be fouled by electrochemical oxidation of phenol in perchlorate (Iniesta et al., 2001). Zhi et al. and Chang et al. also demonstrated the fouling of BDD in the presence of sulfate that proposed possible reaction pathways for phenol electro-oxidation (Zhi et al., 2003; Chang et al., 2006). Kawde et al. reported the influence of glassy carbon electrode surface fouling for phenolic pollutant determination with phosphate electrolyte (Kawde et al., 2013). But there has been few report of electrode fouling caused by organic pollutants in the presence of chloride and insight the effect of active chlorine. Besides that, since the mechanism of electrochemical oxidation is controlled by operating parameters such as current density and anode potential, it will be highly desirable to identify fouling mechanism under different electrochemical conditions. Last, challenges remain in observing the morphology of fouling film on the anode because the pretreatment procedures may cause the morphological damage of fouling structure using scanning electron microscopy (SEM). Therefore, a particular emphasis should be placed on characterization of electrode fouling by using in situ electrochemical measurement and microscopy technology.

The present study mainly focused on characterization of electrode fouling by using in situ electrochemical tests and nondestructive observation of electrode surface in the presence of chloride. First, we carried on the electrochemical analysis to identify the fouling behavior of Pt electrode during electro-oxidation of phenol. Second, the fouling layer on the surface of Pt electrode was identified qualitatively and quantitatively by using in situ nondestructive surface three-dimensional topographies, electrochemical quartz crystal microbalance (EQCM) and Fourier transform infrared spectroscopy (FTIR) measurement. Last, the effect of anions on electrode fouling was discussed during electrochemical indirect oxidation of phenol. The methods developed here for characterizing electrode fouling can be extended to other anode materials not examined here.

2 Materials and methods

2.1 Electrochemical measurements

All the electrochemical measurements were performed using an electrochemical workstation (CHI 760E, CH Instruments Inc., China) with a standard three-electrode system. Experiments were conducted in batch-mode in a 100 mL quartz glass cylindrical electrolytic cell. A Pt foil electrode and stainless steel were used as working electrode and counter electrode, respectively, both with an exposed geometric area of 1 cm^2 that placed vertically in the center of the cell. A single-junction saturated Ag/AgCl electrode was used as the reference electrode. Experiments used 0.1 mol/L sodium chloride (NaCl, Aladdin Reagent Company, China) or 0.1 mol/L sodium sulfate (Na_2SO_4, Aladdin Reagent Company, China) as background electrolyte (pH = 7±0.4) at 25°C. The fouled Pt electrode was obtained during electrochemical reacting with 2.0 mmol/L phenol (C_6H_6O, Tianjin Kermel Chemical Reagent Co. Ltd, China) containing 0.1 mol/L NaCl at 1.0 V vs SHE within 100 min. The cyclic voltammetry (CV) data was recorded between 0.0 and 1.0 V vs SHE with a scan rate of 0.1 V/s. The square wave voltammetry (SWV) was obtained between –0.2 and 1.5 V vs SHE with 25 mV amplitude and 15 Hz frequency. For electrochemical impedance spectroscopy (EIS) measurement, the potential bias was set 1.0 V or 2.7 V vs SHE with a frequency range of 100 kHz to 0.1 Hz. The in situ measurements of Pt electrode mass change were conducted using electrochemical quartz crystal microbalance (EQCM) (QCA922, Princeton, USA). The schematic of electrochemical cell using EQCM measurement was shown in Fig. S1.

2.2 Scanning white-light interferometry for characterization of fouling layer

The fouling layer on Pt electrode surface was observed and measured in situ by using a scanning white light interferometry (SWLI) (NewView 8000, Zygo, USA) based on light interference patterns from a white-light source (Xenon). The SWLI integrated the test results of sub-nanometer film thickness with 3D metrology, and showed imaging of the same area of sample (e.g., 84 μm × 84 μm). The outstanding advantages of SWLI were the in situ, non-contacting, quantitative measurement that avoided damage or contamination of the electrode sample. During the electrochemical oxidation phenol process, the anode samples were observed every 20 min by using SWLI. Other analytical methods were shown in detail in Text S1.

3 Results and discussion

3.1 Electrochemical analysis of electrode fouling

Initially, the SWV was used to investigate the electrode fouling process. As shown in Fig. 1(a), there was no observation of phenol oxidation peak for blank experiment in the absence of phenol. When the phenol (2.0 mmol/L) was added after the second scan, a strong oxidation current (0.47 mA) could be obtained at + 1.03 V vs SHE, indicating direct oxidation of phenol on the electrode surface. However, the unpolished Pt electrode produced a current of 0.16 mA, accounting for 66% decline on the oxidation peak after the uninterrupted third scan. This peak was shifted slightly to more negative potential (+ 0.98 V vs SHE), likely due to the formation of a non-conductive passivating layer on the electrode surface. In the absence of the phenol, re-scanning the same unpolished electrode resulted in disappearance of the oxidation peak, and a new peak of 0.28 mA at 0.05 V vs SHE was observed. These results indicated the formation of stable fouling film on the electrode surface. The electroactive film was likely to be responsible for the formation of a new oxidation peak (Kawde et al., 2013). We further studied the extent to which the anode was fouled by estimating the electrochemically active surface area (ECSA) of Pt electrode based on CV (Fig. 1(b)). According to the method shown in Supporting Information Text S2, the calculations gave the total charges of 1.76×10^{-3} C for pristine Pt electrode (ECSA of 8.38 cm^2) and 3.29×10^{-4} C for fouled Pt electrode (ECSA of 1.57 cm^2), respectively. The 5.33-fold decrease in ECSA clearly suggested inactivation of Pt electrode by fouling layer.

Figure 1(c) shows the chronoamperometric results of direct oxidation of phenol obtained at potential of 1.0 V vs SHE. In this case, the impact of NaCl electrolyte appeared to be slight, as no additional current could be detected after adding 0.1 mol/L NaCl into supporting electrolyte. On the contrary, we observed a sharp increase in current up to 4.0 mA upon the addition of phenol (2.0 mmol/L), followed by a rapid current decay. When we continued to add phenol, no further increase in current could be found, indicating that the Pt electrode surface was almost passivated by fouling layer that prevented electrode from contacting with phenol. The similar phenomena could also be observed when Na_2SO_4 was used as electrolyte (Fig. S2). These results indicated that the anionic species might not exert a major influence on electrode fouling controlled by direct electron transfer oxidation at low potential. We further investigated the electrode fouling using EIS, the technology being useful particularly for the fouling film that was non-conductive (Qader et al., 2019).

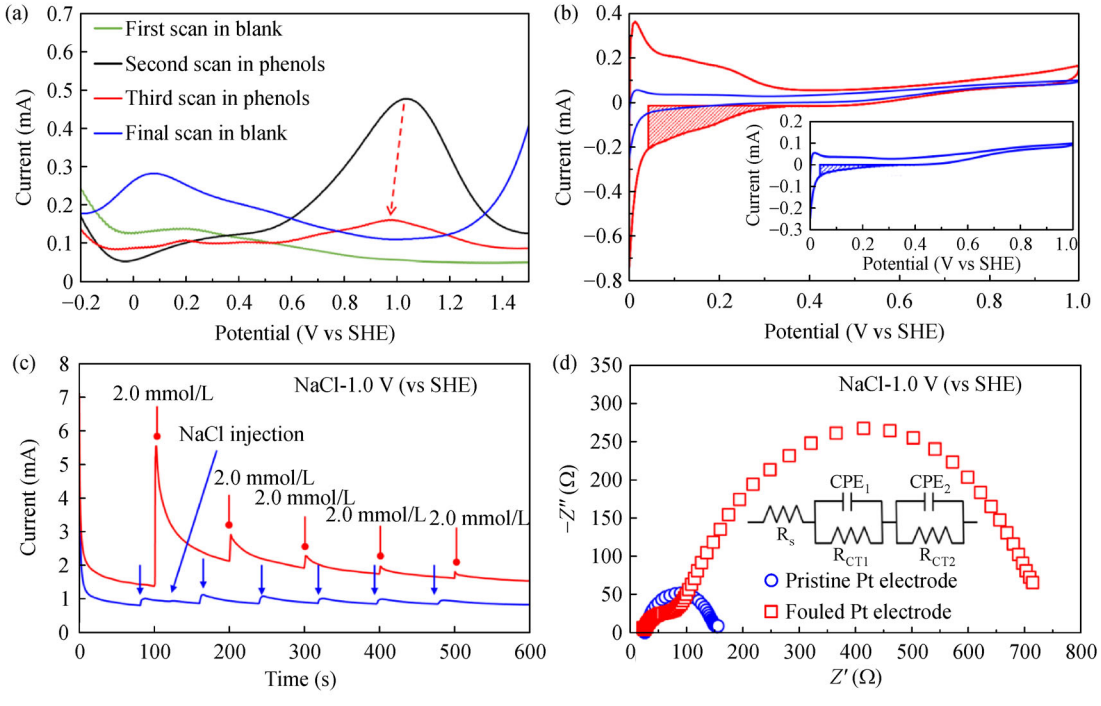

Fig. 1 (a) Square wave voltammetry (SWV) measurements in the presence and absence of 2.0 mmol/L phenol in 0.1 mol/L NaCl supporting electrolyte at pH 6.8±0.5. (b) Cyclic voltammograms (CV) curves of pristine (red line) and fouled (blue line, inset) flat Pt electrode for ECSA measurement in 0.5 mol/L H_2SO_4 supporting electrolyte. (c) Typical chronoamperometric response of Pt electrode to step-by-step injection of phenol containing with 0.1 mol/L NaCl (pH 6.8±0.5) at 1.0 V vs SHE. (d) Nyquist plots of Pt electrode after electrolysis with 2.0 mmol/L phenol in 0.1 mol/L NaCl (pH 6.8±0.5) at 1.0 V vs SHE.

As shown in Fig. 1(d) and Table 1, the EIS curves for fouled Pt electrode had two obvious semicircular loops at high-frequency region (10 MHz) and low-frequency region (173.2 Hz) that represented charge transfer resistance and interface resistance, respectively. This result indicated the formation of a new interface, the fouling layer deposition with 692.8 Ω, between the Pt electrode and electrolyte (Chen et al., 2008). Compared with the new electrode (128.4 Ω), the increased resistance (564.4 Ω) of fouled electrode indicated the increase in charge-transfer resistance of electrode/fouled layer/electrolyte interface.

3.2 Characterization of fouling layer by EQCM and SWLI

The CV curves (Fig. 2(a)) of Pt electrode illustrate the presence of anodic oxidation peak with 10.6 μA current at approximately + 0.96 V vs SHE on the first cycle, and a reduction peak was also found at approximately + 0.46 V vs SHE. To our knowledge, phenol oxidation was an irreversible process, so the reduction peak should be contributed to reduction of Pt surface (Juodkazis et al., 2014). In the subsequent scans, the current finally decreased to 1.3 μA, accounting for 87% decline on the oxidation peak, indicating the formation of stable fouling film on the electrode surface, which was good agreement with the above SWV results. Meanwhile the disappeared reduction peak appeared to declare the same result. The simultaneous mass change responses were recorded by EQCM in Fig. 2(b). The mass increase observed in each forward scan was due to Pt surface oxidation and fouling layer growth, while the mass loss in the backward scan was associated to oxide reduction and anion desorption (Yang et al., 2010). For the second to fourth cycle, their potential and mass variation were similar with in the first cycle shapes, but the mass variation persistently increased by 2.66 μg with four potential cycles according to Sauerbrey

Table 1 Parameters used for fitting the impedance results for the Pt electrodes

Experimental conditions	R_S (Ω)	R_{CT1} (Ω)	CPE_1 (μF)	R_{CT2} (Ω)	CPE_2 (μF)
Prisitne Pt electrode	20.38	128.4	102.3	–	–
1.0 V (vs SHE) with NaCl	21.12	109	126.2	692.8	235.1
2.7 V (vs SHE) with Na_2SO_4	27.17	22.5	33.9	146.1	130.7
2.7 V (vs SHE) with NaCl	25.42	125.8	121.6	–	–

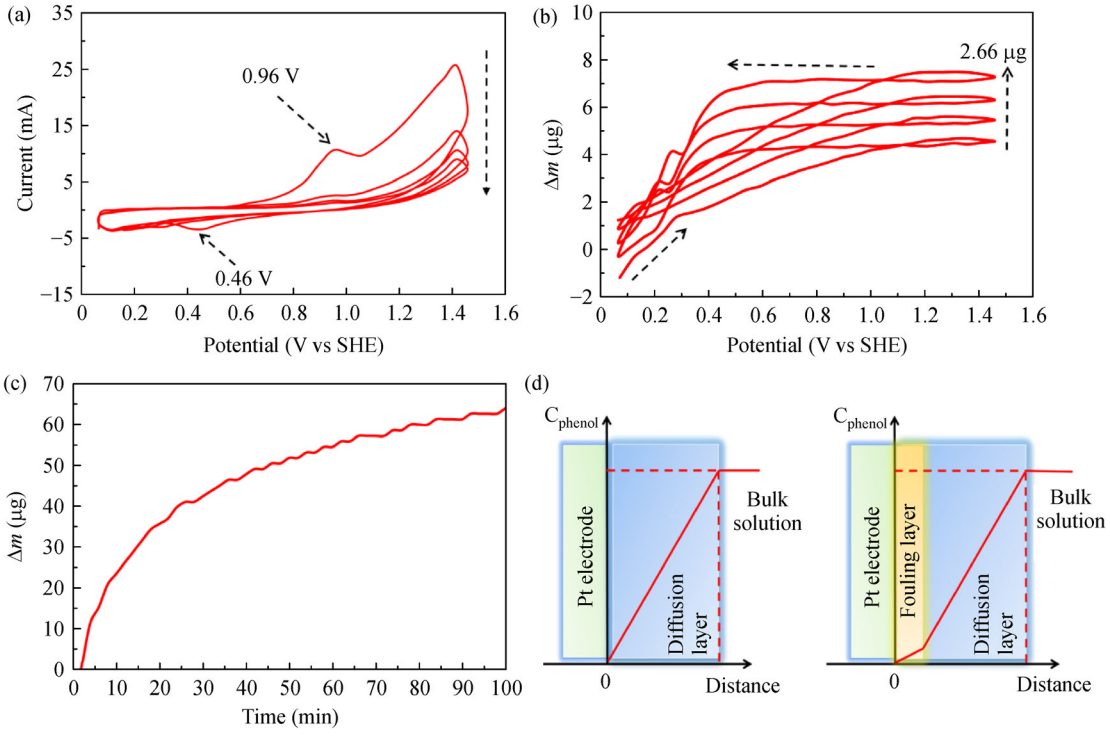

Fig. 2 (a) CV curves and (b) mass change during CV test for 2.0 mmol/L phenol in 0.1 mol/L NaCl supporting electrolyte. (c) Mass change of Pt electrode during electrolysis of 2.0 mmol/L phenol in 0.1 mol/L NaCl at 1.0 V vs SHE. (d) Schematic illustration of concentration profile of phenol close to the electrode surface.

equation (Supporting Information Text S3). Moreover, the surface mass of Pt electrode (Fig. 2(c)) increased 63.9 μg during 100 min electrochemical reacting that was a strong evidence for the fouling layer growth. Figure 2(d) shows the simplified concentration profile of phenol being close to the electrode surface. The presence of a fouling layer could act as a barrier to prevent contact between pollutants and electrode surface to affect electrochemical oxidation.

To get access to in situ observation of fouling film growing in Pt electrode surface, we used SWLI to record the change of morphology of electrode in Fig. 3. SWLI is a power technique for providing three-dimensional metrology of surface with a vertical resolution of 0.01 nm. More importantly, there is no damage to morphology of the tested surface because of noncontacting measurement. As the defect sites on the electrode surface are non-electroactive (Meng et al., 2017), the thickness of defect sites is defined as the base plane (δ = 0 nm), against which the thickness of fouling film (δ) growing on the non-defect surface is measured and recorded. Figure S3 shows the base plane of defect sites of all the electrode samples with areas in blue color. With electrolysis of 100 min, the fouling film was growing gradually on the Pt electrode surface, indicated by the stepwise increase in surface roughness and concurrent increase in thickness of film from δ = 0.41 μm (0–20 min), to δ = 0.56 μm (20–40 min), δ = 0.37 μm (40–60 min), δ = 0.57 μm (60–80 min) and finally δ = 0.40 μm (80–100 min). This clearly indicated the deposition of fouling film growing on electrode during electrolysis. Further electrochemical reaction tended to the formation of denser and thicker film that uniformly covered the Pt electrode surface. As shown in Fig. S4, the thickness of fouling film was positively related to electrolysis time, reaching the maximum of δ = 2.31 μm at the end of 100 min. This is in good agreement with the results obtained from EQCM measurement, accounting for the increase in mass to m = 63.9 μg on of Pt electrode (0.196 cm^2; Fig. 2(c)). Then the corresponding rate at which the mass of fouling layer increased (k) was estimated to be 3.26 μg/cm^2/min. Based on δ = 2.31 μm, surface density of 326.0 μg/cm^2 and geometric anode area of 1.0 cm^2, the volumetric density of fouling film on average could be estimated to be 1.41 g/cm^3. This value appeared to be in line with the density of organic polyphenol-like substances such as poly tannic acid and poly pyrogallol whose volumetric density was in the range of 1.30–1.59 g/cm^3 (Sousa et al., 2018; Wu et al., 2019).

3.3 Characterization of functional groups of fouling layer by FTIR

Next, FTIR was used to characterize the functional groups

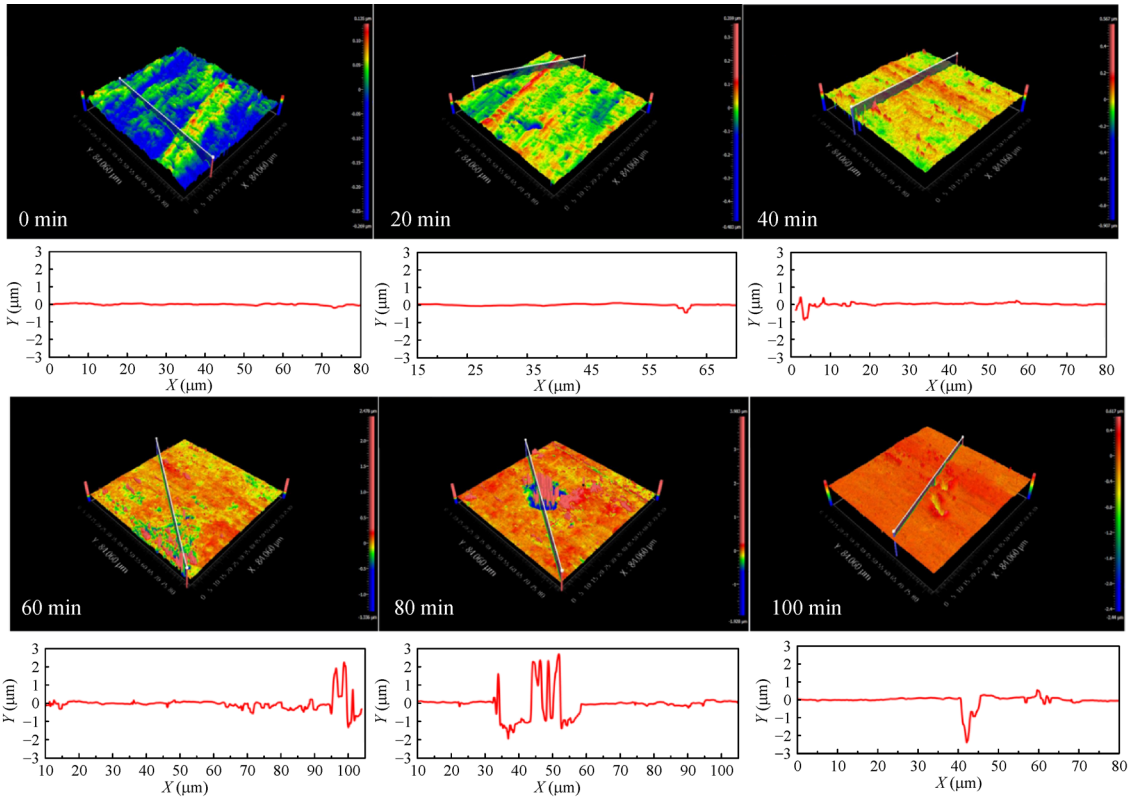

Fig. 3 Time course of 3D topographies of Pt electrode surface and surface height curves during electrolysis of 2.0 mmol/L phenol in 0.1 mol/L NaCl electrolyte at 1.0 V vs SHE within 100 min.

involved in the fouling layer. As illustrated in Fig. 4, the peak strength of all the functional groups detected was increased with electrolysis time from 0 min to 100 min, indicating temporal growth of fouling layer on Pt electrode. The appearance of quinone groups with a characteristic C = O vibration at wavelength of 1640–1660 cm^{-1} should be assinged to the polyphenol produced from direct oxidation or indirect oxidation of phenol by intermediates (Hawkridge and Pemberton, 2003). The characteristic peaks at 1579 cm^{-1} and 1490 cm^{-1} represented the aromatic C-C stretching vibrations, corresponding to the polyphenol related to polyester with the benzene rings contacted by C-C links (Gattrell and Kirk, 1992). The strong peak located at 1214 cm^{-1} corresponded C-O stretching vibration, indicating that the polymer was composed of polyphenol because of the aromatic ether chain structure (Ežerskis and Jusys, 2001). It provided another possibility that structure of polymer. In addition, the peak found at 834 cm^{-1} was attributed to a C-H stretching vibration, and peaks at 755 cm^{-1} and 693 cm^{-1} could be relative to the oxidative intermediate products of phenol (Volkov et al., 1980) such as pyrocatechol and hydroquinone. As illustrated schematically in Fig. S5, when a positive potential is applied, the phenate anions transfer one electron to anode with the formation of phenol radicals that can further combine with each other to generate phenoxy phenol or dihydroxyl benzene (Volkov et al., 1980; Zhi et al., 2003). It is assumed that both dimers remain to have the characteristics of phenol to follow the same oxidation route until the coating layer covers the anode surface (Iniesta et al., 2001; Ferreira et al., 2006; Bao et al., 2010).

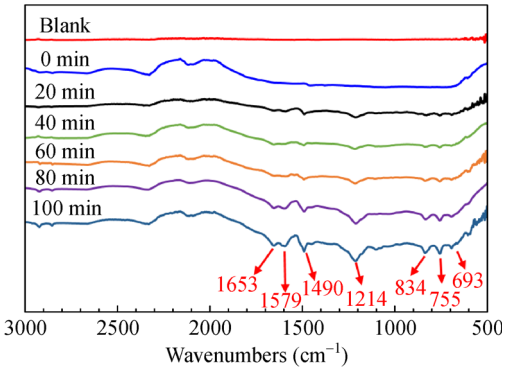

Fig. 4 FTIR spectra during electrolysis of 2.0 mmol/L phenol in 0.1 mol/L NaCl electrolyte at 1.0 V vs SHE within 100 min.

3.4 Effect of chloride on electrode fouling

We examined the effect of electrolyte (i.e., NaCl and Na_2SO_4) on electrode fouling during electrochemical oxidation at potential of 2.7 V (vs SHE), the potential sufficiently high for electrolysis of water and chloride. As shown in Figs. 5(a) and 5(b), the electrode fouling behaved in a completely different manner for NaCl and Na_2SO_4 electrolyte. The increased current was seen to be always related to addition of phenol in the presence of NaCl. On the contrary, during the electrolysis in the absence of chloride, the current was found to increase persistently to a stable level until the third-cycle phenol addition. The ongoing addition of phenol led to a gradual decrease in the current from 26.4 mA to 24.4 mA within a time of 400 s and the Pt electrode was no longer sensitive to concentration of phenol, suggesting that the electrode surface was passivated by phenol. The charge-transfer resistance of Pt electrode was almost unchangeable (125.8 Ω; Fig. 5(c) and Table 1), indicating no formation of fouling film in the presence of chloride at potential higher than 2.7 V (vs SHE). In comparison, owing to the absence of chloride, the interfacial resistance (R_{CT2}) caused by fouling layer was 146.1 Ω, a value 13.9% greater than that in the presence of chloride (Fig. 5(d)). The FTIR spectra also confirmed these results shown in Fig. S6 because of the difference in functional groups on anode surface after oxidation in NaCl and Na_2SO_4. The two likely explanations for this discrimination should be the role of the formation of gas (O_2 and Cl_2) or the production of active species responsible for damage of polymeric fouling layer formed by electrochemical polymerization of phenol.

To verify above hypothesis, the role of the formation of gas was further discussed. The oxygen evolution potential and chlorine evolution potential of Pt were observed at 1.35 V and 1.42 V (vs SHE) in Fig. S7(a). Thus, the experiments were conducted at 1.7 V vs SHE that potential could only produce gas without active species. Figure S7 (b) observed that the results were similar to that of low potential (1.0 V) direct oxidation, indicating that the generation of chlorine or oxygen could not effectively prevent the electrode fouling. This indirectly supported that active species were responsible for damage of polymeric fouling layer during indirect oxidation. Furthermore, the XPS analysis was carried out to examine the surface chemical compositions and valence states of Pt electrode during electrolysis. As shown in Fig. 6(a), the strong peaks located at binding energy of 74.8 eV and 71.5 eV was assigned to metallic Pt. Following electrolysis in NaCl electrolyte, additional characteristic peaks appeared at binding energy of 72.0 eV and 75.5 eV (Pt^{2+}) and a weak peak at 78.0 eV (Pt^{4+}) (Fig. 6(b)) (Li et al., 2013). Significantly, the characteristic peak of Cl at binding energy of 199.8 eV was observed on the electrode surface after repeated cleaning (Fig. 6(c)). The XPS spectra displayed the similar results in Na_2SO_4 electrolyte except for chlorine in Fig. S8. This experimentally confirmed the electrochemical formation of chloride complexes in chloride-containing electrolyte on the Pt electrode according to Eqs. (1) and (2) (Li et al., 2011)

$$Pt + 4Cl^- \rightarrow PtCl_4^{2-} + 2e^-$$

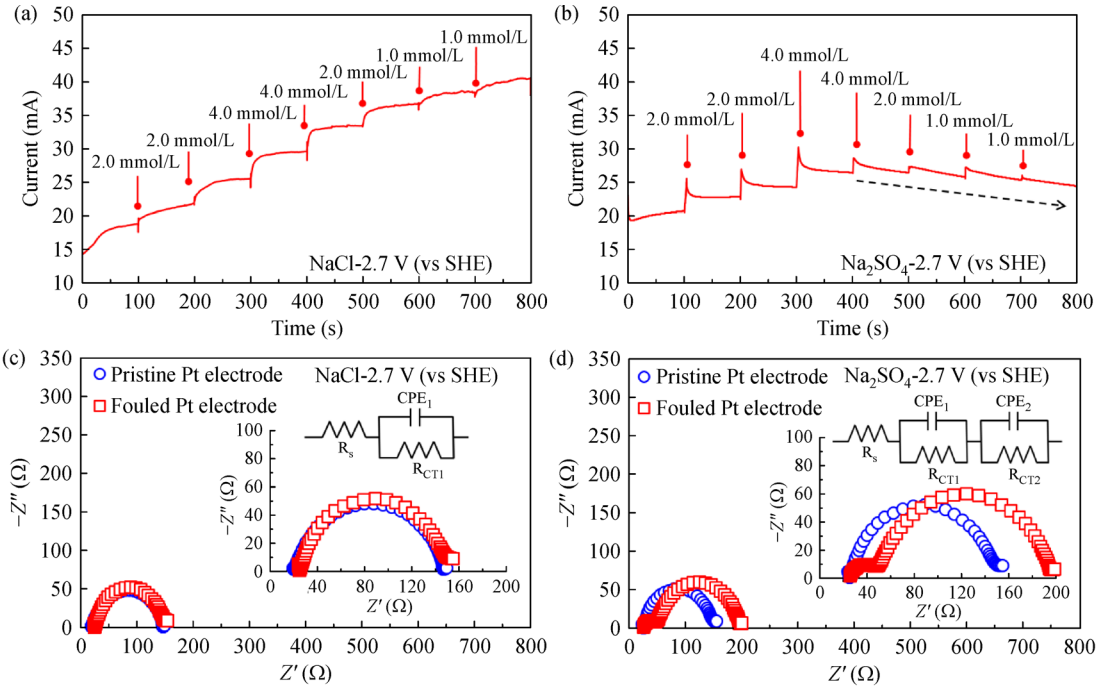

Fig. 5 Chronoamperometric response of Pt electrode to step-by-step injection of phenol at 2.7 V vs SHE in (a) 0.1 mol/L NaCl and (b) 0.1 mol/L Na_2SO_4. Nyquist plots of Pt electrode after electrolysis of 2.0 mmol/L phenol in (c) 0.1 mol/L NaCl and (d) 0.1 mol/L Na_2SO_4 at 2.7 V vs SHE.

$$E^0 = 0.758\text{V(vs.SHE)} \quad (1)$$

$$\text{Pt} + 6\text{Cl}^- \rightarrow \text{PtCl}_6^{2-} + 4\text{e}^-$$

$$E^0 = 0.742\text{V (vs.SHE)} \quad (2)$$

In comparison, the reaction in chloride-free electrolyte might be described as Eqs. (3) and (4) (Arslan et al., 2005).

$$\text{Pt} + \text{H}_2\text{O} \rightarrow \text{PtO} + 2\text{H}^+ + 2\text{e}^-$$

$$E^0 = 0.98\text{V (vs.SHE)} \quad (3)$$

$$\text{PtO} + \text{H}_2\text{O} \rightarrow \text{PtO}_2 + 2\text{H}^+ + 2\text{e}^-$$

$$E^0 = 1.045\text{V (vs.SHE)} \quad (4)$$

In reality, Pt electrode tended to react with chloride other than with water, preliminarily due to the lower redox potential required for chlorine evolution and chlorination. In addition, the strong adsorption of chloride on the electrode surface might retard the electrochemical reaction between water and Pt.

We next examined the active species by using DMPO as a spin trap agent followed by ESR measurement. As shown in Fig. 6(d), there was no observation of definable ESR peak of DMPO-adduct at low potential (1.0 V vs SHE) with and without chloride, indicating the thermodynamic impossibility of both oxygen (1.23 V vs SHE) and chlorine evolution (1.36 V vs SHE). The samples collected from higher potential (2.7 vs SHE) without chloride yielded quartet lines with peak strength of 1:2:2:1, which clearly indicated typical signals of DMPO-OH adduct and thus OH• formation (Jiang et al., 2016; Lu et al., 2020). Notably, the seven-line ESR peaks were seen in the presence of chloride, which provided an experimental verification for the formation of Cl• radicals as the main intermediate active species (Li et al., 2016). Based on external standard agent TEMPOL (Fig. S9), OH• and Cl• radicals concentration could be quantified as 43.7 μmol/L and 40.4 μmol/L. According to previous reports, OH• is a non-selective strong oxidant that reacts with organic moieties at the rate constants being close to diffusion-controlled rates (Lee and von Gunten, 2010). However, Cl• belongs to an oxidant that is more selective to react only with electron-rich moieties via single-electron transfer oxidation, H-abstraction, addition to unsaturated C-C bonds, and attacking active sites of organic polymer (Grebel et al., 2010). Therefore, this may provide the most likely explanation to the reason why the presence of chloride ions allow the mitigation of electrode fouling at higher potential.

3.5 Implications

This study provides a demonstration of electrode fouling in the solution containing phenol and chloride. The electro-

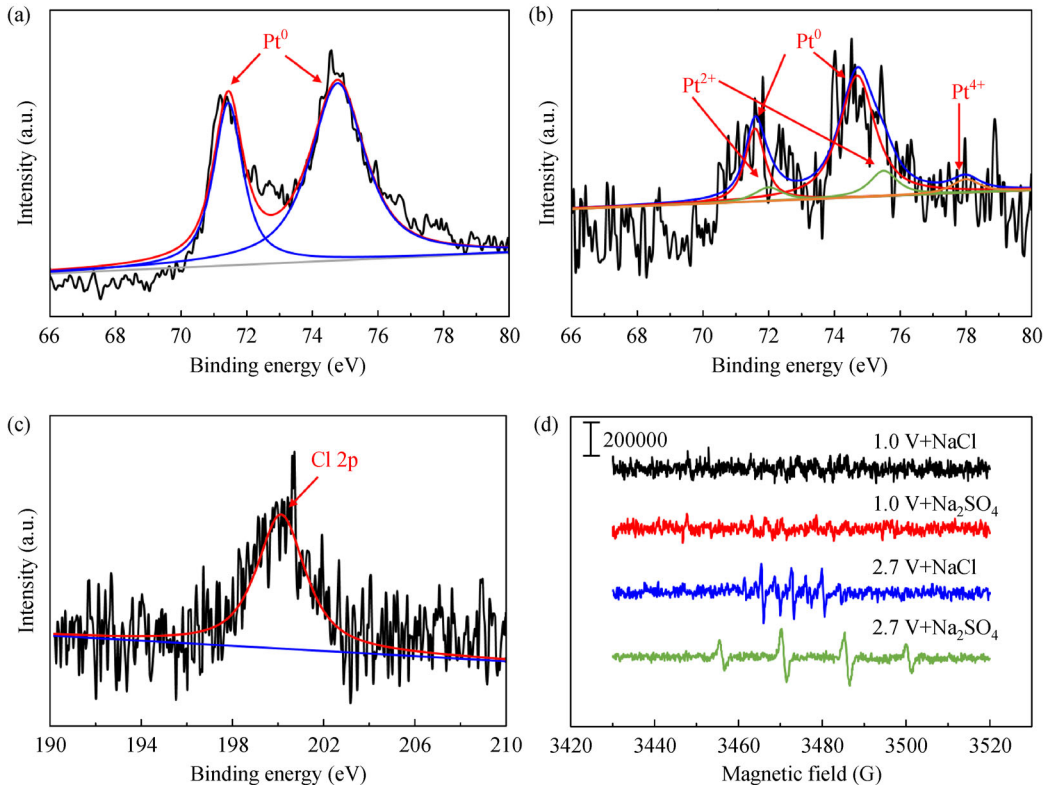

Fig. 6 High-resolution XPS spectra of (a) pristine and (b) fouled Pt electrode, and (c) Cl 2p after electrolysis of 2.0 mmol/L phenol in 0.1 mol/L NaCl electrolyte at 2.7 V vs SHE. (d) ESR spectra with DMPO serving as trapping agent after 10 min electrolysis.

oxidation of phenol proceeded via direct electron transfer process in the potential region of water stability (1.0 V vs SHE) on Pt surface, which resulted in electrode fouling caused by the formation of polymeric film. The direct electro-oxidation was found to be less dependent on anions in the electrolyte. In the presence of chloride, the electrode fouling caused by direct oxidation could be addressed by applying higher potential (2.7 V vs SHE) under which the active chlorine was produced (Cl·). Lower potential appeared to accelerate the electro-polymerization process because the generation of phenol radicals was much easier than that at high potential. Dimer of phenoxy phenol had the lowest steric hindrance, making it easily couple with other active species. In reality, the electrode fouling is a very complex process that may be influenced by several factors such as the nature of electrode, organic pollutants, working potential and the type and concentration of anions. Within this context, this study suggests the macro-scale mechanisms of electrode fouling, and thus offers a possibility to optimize operating parameters to prevent the electrode fouling. In addition to Pt electrode, we also preliminarily tested Ti_4O_7, PbO_2 and Ti/RuO_2 serving as anode for electrode fouling research by typical chron-oamperometric response. As shown in Fig. S10, the various electrodes may have different current response to pollutants due to the otherness of internal structure (plate or porous) or electrochemistry performance. But anyway, the electrodes always have the trend of being fouled during the direct oxidation. Therefore, the methodology reported in this study may be also available for further investigating the fouling of other types of anode material in electro-oxidation process to better treating more complex realistic wastewater.

4 Conclusions

The present study demonstrated the electrode fouling during electro-oxidation water purification by using in situ electrochemical measurements and non-destructive observation of the electrode morphology, and the major conclusions could be drawn as follows. The electrode fouling was highly dependent on thermodynamic process of electrode that was controlled by anode potential. At anode potential lower than 1.0 V vs SHE, the direct electro-oxidation caused the electrode fouling by the formation of polymeric film. The degree to which the anode was fouled was independent of anion in the electrolyte. In comparison, at anode potential higher than 2.7 V vs SHE, the anions (e.g., chloride) could exert a major influence to the behavior of electrode fouling. The presence of chloride was shown to mitigate the fouling of electrode significantly through preventing the formation of polymeric film by active chlorine (e.g., Cl• and Cl_2)

produced from anodic oxidation of chloride. Since chloride is the most abundant anionic species existing in both natural and engineered water system, this study not only offers a deep insight into the mechanism of electrode fouling, but also suggests strategies for anti-fouling in the presence of chloride in electro-oxidation process. The methods developed here are also available for characterizing the electrode fouling of other anode materials not examined in this study.

Acknowledgements Project was supported by the National Natural Science Foundation of China (Grant Nos. 51822806, 51678184, 51671117, and 51761145031), the Fundamental Research Funds for the Central Universities (No. HIT.BRETIV.201905), and the State Key Laboratory of Urban Water Resource and Environment (Harbin Institute of Technology) (No. 2020DX07).

Electronic Supplementary Material Supplementary material is available in the online version of this article at https://doi.org/10.1007/s11783-020-1345-7 and is accessible for authorized users.

References

Almeida L C, Silva B F, Zanoni M V B (2015). Photoelectrocatalytic/Photoelectro-Fenton coupling system using a nanostructured photoanode for the oxidation of a textile dye: Kinetics study and oxidation pathway. Chemosphere, 136: 63–71

Arslan G, Yazici B, Erbil M (2005). The Effect of pH, temperature and concentration on electrooxidation of phenol. Journal of Hazardous Materials, 124(1–3): 37–43

Bao L Y, Xiong R C, Wei G (2010). Electrochemical polymerization of phenol on 304 stainless steel anodes and subsequent coating structure analysis. Electrochimica Acta, 55(12): 4030–4038

Barhoumi N, Olvera-Vargas H, Oturan N, Huguenot D, Gadri A, Ammar S, Brillas E, Oturan M A (2017). Kinetics of oxidative degradation/mineralization pathways of the antibiotic tetracycline by the novel heterogeneous electro-Fenton process with solid catalyst chalcopyrite. Applied Catalysis B: Environmental, 209: 637–647

Barhoumi N, Oturan N, Olvera-Vargas H, Brillas E, Gadri A, Ammar S, Oturan M A (2016). Pyrite as a sustainable catalyst in electro-Fenton process for improving oxidation of sulfamethazine. Kinetics, mechanism and toxicity assessment. Water Research, 94: 52–61

Chang C C, Chen L C, Liu S J, Chang H C (2006). Investigation of electro-oxidation of methanol and benzyl alcohol at boron-doped diamond electrode: Evidence for the mechanism for fouling film formation. Journal of Physical Chemistry B, 110(39): 19426–19432

Chen L C, Chang C C, Chang H C (2008). Electrochemical oxidation of histidine at an anodic oxidized boron-doped diamond electrode in neutral solution. Electrochimica Acta, 53(6): 2883–2889

Ežerskis Z, Jusys Z (2001). Electropolymerization of chlorinated phenols on a Pt electrode in alkaline solution Part I: A cyclic voltammetry study. Journal of Applied Electrochemistry, 31(10): 1117–1124

Ferreira M, Varela H, Torresi R M, Tremiliosi-Filho G (2006). Electrode passivation caused by polymerization of different phenolic compounds. Electrochimica Acta, 52(2): 434–442

Gao G D, Vecitis C D (2012). Doped carbon nanotube networks for electrochemical filtration of aqueous phenol: Electrolyte precipitation and phenol polymerization. ACS Applied Materials & Interfaces, 4(3): 1478–1489

Gattrell M, Kirk D W (1993). A study of electrode passivation during aqueous phenol electrolysis. Journal of the Electrochemical Society, 140(4): 903–911

Grebel J E, Pignatello J J, Mitch W A (2010). Effect of halide ions and carbonates on organic contaminant degradation by hydroxyl radical-based advanced oxidation processes in saline waters. Environmental Science & Technology, 44(17): 6822–6828

Hawkridge A M, Pemberton J E (2003). Model aluminum-poly (p-phenylenevinylene) interfaces studied by surface Raman spectroscopy. Journal of the American Chemical Society, 125(3): 624–625

Hou Y P, Peng Z B, Wang L, Yu Z B, Huang L R, Sun L F, Huang J (2018). Efficient degradation of tetrabromobisphenol a via electrochemical sequential reduction-oxidation: Degradation efficiency, intermediates, and pathway. Journal of Hazardous Materials, 343: 376–385

Iniesta J, Michaud P A, Panizza M, Cerisola G, Aldaz A, Comninellis Ch (2001). Electrochemical oxidation of phenol at boron-doped diamond electrode. Electrochimica Acta, 46(23): 3573–3578

Jiang C J, Liu L F, Crittenden J C (2016). An electrochemical process that uses an Fe^0/TiO_2 cathode to degrade typical dyes and antibiotics and a bio-anode that produces electricity. Frontiers of Environmental Science & Engineering, 10(4): 15–22

Juodkazis K, Juodkazytė J, Šebeka B, Juodkazis S (2014). Reversible hydrogen evolution and oxidation on Pt electrode mediated by molecular ion. Applied Surface Science, 290: 13–17

Kawde A, Morsy M A, Odewunmi N, Mahfouz W (2013). From electrode surface fouling to sensitive electroanalytical determination of phenols. Electroanalysis, 25(6): 1547–1555

Lee Y, von Gunten U (2010). Oxidative transformation of micropollutants during municipal wastewater treatment: Comparison of kinetic aspects of selective (chlorine, chlorine dioxide, ferrateVI, and ozone) and mon-selective oxidants (hydroxyl radical). Water Research, 44(2): 555–566

Li H, Wang H J, Qian W M, Zhang S S, Wessel S, Cheng T T H, Shen J, Wu S H (2011). Chloride contamination effects on proton exchange membrane fuel cell performance and durability. Journal of Power Sources, 196(15): 6249–6255

Li S H, Zhao Y, Chu J, Li W W, Yu H Q, Liu G, Tian Y C (2013). A Pt-Bi bimetallic nanoparticle catalyst for direct electrooxidation of formic acid in fuel cells. Frontiers of Environmental Science & Engineering, 7(3): 388–394

Li T, Jiang Y, An X Q, Liu H J, Hu C, Qu J H (2016). Transformation of humic acid and halogenated byproduct formation in UV-chlorine processes. Water Research, 102: 421–427

Lu C, Deng K L, Hu C, Lyu L (2020). Dual-reaction-center catalytic process continues Fenton's story. Frontiers of Environmental Science & Engineering, 14(5): 82

Martínez-Huitle C A, Ferro S (2006). Electrochemical oxidation of organic pollutants for the wastewater treatment: Direct and indirect processes. Chemical Society Reviews, 35(12): 1324–1340

Meng Q F, Cai K F, Chen Y X, Chen L D (2017). Research progress on conducting polymer based supercapacitor electrode materials. Nano Energy, 36: 268–285

Qader B, Baron M, Hussain I, Sevilla J M, Johnson R P, Gonzalez-Rodriguez J (2019). Electrochemical determination of disulfoton using a molecularly imprinted poly-phenol polymer. Electrochimica Acta, 295: 333–339

Qi Z L, You S J, Liu R B, Chuah C J (2020). Performance and mechanistic study on electrocoagulation process for municipal wastewater treatment based on horizontal bipolar electrodes. Frontiers of Environmental Science & Engineering, 14(3): 40

Sousa A M L, Li T D, Varghese S, Halling P J, Aaron Lau K H (2018). Highly active protein surfaces enabled by plant-based polyphenol coatings. ACS Applied Materials & Interfaces, 10(45): 39353–39362

Tang T L, Yan W, Zheng C L (2014). Electrochemical oxidation of humic acid at the antimony- and nickel-doped tin oxide electrode. Frontiers of Environmental Science & Engineering, 8(3): 337–344

Volkov A, Tourillon G, Lacaze P C, Dubois J E (1980). Electrochemical polymerization of aromatic amines: IR, XPS and PMT study of thin film formation on a Pt electrode. Journal of Electroanalytical Chemistry and Interfacial Electrochemistry, 115(2): 279–291

Wang X Y, Xie Y, Yang G Z, Hao J M, Ma J, Ning P (2020). Enhancement of the electrocatalytic oxidation of antibiotic wastewater over the conductive black carbon-PbO_2 electrode prepared using novel green approach. Frontiers of Environmental Science & Engineering, 14(2): 22

Wu L P, Shao H, Fang Z H, Zhao Y C, Cao C Y, Li Q L (2019). Mechanism and effects of polyphenol derivatives for modifying collagen. ACS Biomaterials Science & Engineering, 5(9): 4272–4284

Xiao M S, Zhang Y G (2016). Electro-catalytic oxidation of phenacetin with a three-dimensional reactor: Degradation pathway and removal mechanism. Chemosphere, 152: 17–22

Xu D, Li Y, Yin L F, Ji Y Y, Niu J F, Yu Y X (2018). Electrochemical removal of nitrate in industrial wastewater. Frontiers of Environmental Science & Engineering, 12(1): 9

Yang Q, Zhang Y Y, Li H T, Zhang Y Q, Liu M L, Luo J, Tan L, Tang H, Yao S Z (2010). Electrochemical copolymerization study of o-toluidine and o-aminophenol by the simultaneous EQCM and in situ FTIR spectroelectrochemisty. Talanta, 81(1–2): 664–672

Zhi J F, Wang H B, Nakashima T, Rao T N, Fujishima A (2003). Electrochemical incineration of organic pollutants on boron-doped diamond electrode. Evidence for direct electrochemical oxidation pathway. Journal of Physical Chemistry B, 107(48): 13389–13395